Volume Registration Using the 3-D Pseudopolar Fourier Transform

Yosi Keller, Yoel Shkolnisky, and Amir Averbuch

***Abstract*—This paper introduces an algorithm for the registration of rotated and translated volumes using the three-dimensional (3-D) pseudopolar Fourier transform, which accurately computes the Fourier transform of the registered volumes on a near-spherical 3-D domain without using interpolation. We propose a three-step procedure. The first step estimates the rotation axis. The second step computes the planar rotation relative to the rotation axis. The third step recovers the translational displacement. The rotation estimation is based on Euler's theorem, which allows one to represent a 3-D rotation as a planar rotation around a 3-D rotation axis. This axis is accurately recovered by the 3-D pseudopolar Fourier transform using radial integrations. The residual planar rotation is computed by an extension of the angular difference function [1] to cylindrical motion. Experimental results show that the algorithm is accurate and robust to noise.**

***Index Terms*—Non-Carlesian FFT, pseudopolar FFT, volume registration.**

I. Introduction

RIGID volume registration is a major component in three-dimensional (3-D) object modeling in a diverse range of applications. Examples for such applications are the assembly of 3-D models from complementary patches [2]–[4], range imaging [5], and bioinformatics [6], [7]. Let $V_1(\vec{x})$ and $V_2(\vec{x})$, $\vec{x} = (x, y, z)$, be two partially overlapping volumes that are related by a 3-D rigid transformation

$$V_1(\vec{x}) = V_2(R\vec{x} + \Delta\vec{x}) \tag{1.1}$$

where R is a 3-D rotation matrix and $\Delta\vec{x} = (\Delta x, \Delta y, \Delta z) \in \mathbb{R}^3$. The goal of the registration process is to estimate R and $\Delta\vec{x}$.

There are several approaches towards 3-D registration, that can be categorized as either feature or intensity based. Feature-based approaches [3], [8]–[10] detect a set of features in the registered volumes and align the volumes by using the coordinates of these features. Intensity-based schemes [6], [11] align the volumes by using the intensities of the voxels.

Intensity-based algorithms include optimization- and Fourier-based schemes. Optimization-based schemes formulate the registration problem as the optimization of some cost function, such as the L_2 norm [12], and then use a general-purpose optimization algorithm to optimize the cost function. Reference [12] extends the widely used gradient methods to 3-D image registration. It uses Newton's method to minimize the L_2 norm of the intensity differences as a function of motion parameters. Due to the properties of nonlinear optimization, these algorithms are unable to estimate large motions. To estimate large motions, such schemes are used in conjunction with a bootstrapping method, which computes a prealignment that is close to the optimum.

Frequency-domain methods are of particular relevance to this paper. These methods use the properties of the Fourier transform to separately estimate rotation and translation. This reduces a problem with six degrees of freedom into two problems with three degrees of freedom (see [11] and [13] as examples for these methods). The algorithm in [11] consists of three steps. The first recovers the rotation axis, the second recovers the rotation angle, and the third recovers the translation parameters. To recover the rotation parameters, the algorithm normalizes the Fourier transform of the input objects and integrates it in the radial direction. The direction in which this integral is minimal is the direction of the rotation axis. The polar Fourier coefficients are interpolated from the Cartesian Fourier coefficients. As this task is computationally intensive, the entire set of polar coefficients cannot be computed directly. Thus, simulated annealing is used to find the minimum of the integral. Simulated annealing might not converge to the global minimum, and the performance of such algorithms in terms of speed and accuracy cannot be estimated. This renders such approaches prohibitive for time-critical applications, or applications where the accuracy must be predictable. Furthermore, the integration in the radial direction suffers from inaccuracies caused by discretization and interpolation errors, and therefore, such schemes cannot achieve high accuracy. The planar rotation is recovered using a scheme similar to [14], where again, interpolating the Fourier coefficients results in inaccuracies and high computational complexity. Once the rotation parameters are recovered, the translation is recovered using phase correlation [15].

Another frequency-domain approach is given in [13]. This algorithm recovers the rotation parameters by formulating the problem as a linear system, whose entries are computed by the frequency-domain relations of the two objects. As before, the translation parameters are recovered by using phase correlation. As in [11], the algorithm requires integration in the radial direction, which incurs inaccuracies. The method proposed in this paper outperforms the method in [11].

The 3-D spherical Fourier transform is used in [7] for protein–protein docking. The density volumes are aligned by computing the magnitude of their polar Fourier transform. As the volumes are given on Cartesian grids, the polar Fourier

Manuscript received March 13, 2005; accepted February 1, 2006. The work of Y. Shkolnisky was supported by the Ministry of Science, Israel, under a grant. The associate editor coordinating the review of this manuscript and approving it for publication was Dr. Hilde M. Huizenga.

Y. Keller is with the Mathematics Department, Yale University, New Haven, CT 06511 USA (e-mail: yosi.keller@yale.edu).

Y. Shkolnisky and Amir Averbuch are with the School of Computer Science, Tel Aviv University, Tel Aviv 69978, Israel (e-mail: yoel@math.tau.ac.il; amir@math.tau.ac.il).

Color versions of Figs. 1, 2, and 5 are available online at http://ieeexplore.ieee.org.

Digital Object Identifier 10.1109/TSP.2006.881217

transform is interpolated from the Cartesian 3-D Fourier transform coefficients. Thus, rotations are reduced to translations in the spherical coordinate system that are recovered by applying phase correlation [15]. The residual translation is also estimated by phase correlation.

A different computational approach is suggested in [16]. It uses an extension of spherical harmonics to compute a two-dimensional (2-D) Fourier transform of a restriction of the registered volumes to the surface of a sphere. These are used to evaluate the correlation function of the registered volumes in spherical coordinates. In contrast, the previously mentioned schemes [7], [11] (as well as ours) use 3-D Fourier transforms. The work in [16] deals with pure rotations, and by using the spherical harmonics representation, rotations are reduced to translations that can be efficiently recovered. Moreover, the assumption of pure rotation allows the correlation function to include the phase information that is often ignored when translations are also considered.

This scheme is extended in [6] to handle both rotations and translations and is successfully applied to the docking of atomic structures (density maps). The alignment problem is reformulated using five rotation angles and a single translation parameter. The maximum of the correlation function in the five-dimensional space is efficiently detected by computing the spherical harmonics in a five-dimensional space.

In this paper, we extend the preliminary results given in [17]. We present a Fourier-based approach that does not require interpolation in the frequency domain. It is based on the 2-D pseudopolar Fourier transform (PPFT2D) [18] and 3-D pseudopolar Fourier transform (PPFT3D) [19], which compute the discrete Fourier transform (DFT) on non-Cartesian grids. This allows a fast and algebraically accurate registration, which draws on Euler's theorem to estimate the 3-D rotation. The algorithm has three steps. First, the 3-D pseudopolar Fourier transform is used to recover the rotation axis. Then, the rotation around the axis is estimated using a pseudocylindrical representation computed with the 2-D pseudopolar Fourier transform. Finally, the translation is computed by using phase correlation [15].

We provide an algorithm that is both efficient and mathematically rigorous. The scheme efficiently and accurately computes the radial integration; hence, the execution time and accuracy of the algorithm are predictable and depend only on the size of the input volumes. In particular, the algorithm does not use general-purpose optimization techniques, whose performance depends on the content of the input volumes. Therefore, the complexity of the algorithm is of the same order as the 3-D fast Fourier transform (FFT). The second step in our scheme is based on an extension of the image registration scheme given in [1]. We extend it to handle cylindrical geometry, that is, the estimation of the relative 2-D rotations of a set of planes around a common axis. Unlike [11] and [14], it is fast, noniterative, does not use interpolation, guarantees convergence in a predictable time regardless of the volume's content, and has a predictable registration error.

The proposed scheme accurately estimates arbitrary large rotations without applying a general-purpose optimization scheme (gradient based, simulated annealing, etc.). The only "optimization" required is finding the minimal element in an array. It is fast, robust to noise, and the registration accuracy can be increased arbitrarily. The implementation requires only one-dimensional (1-D) operations and is therefore appropriate for real-time implementations.

This paper is organized as follows. Sections II and III present the 3-D pseudopolar Fourier transform and apply Euler's theorem to 3-D rotations, respectively. Planar rotations are recovered in Section IV, and Section V describes the estimation of translations. Experimental results and concluding remarks are given in Sections VI and VII, respectively.

II. 3-D Pseudopolar Fourier Transform

Given a volume I of size $N \times N \times N$, its 3-D Fourier transform, denoted $\hat{I}(\omega_x, \omega_y, \omega_z)$ or $\mathcal{F}(I)$, is given by

$$\begin{aligned}\hat{I}(\omega_x,\omega_y,\omega_z) &= \mathcal{F}(I)(\omega_x,\omega_y,\omega_z)\\ &= \sum_{u,v,w=-N/2}^{N/2-1} I(u,v,w) e^{-\frac{2\pi i}{M}(u\omega_x+v\omega_y+w\omega_z)},\\ &\quad \omega_x,\omega_y,\omega_z \in \mathbb{R}. \end{aligned} \tag{2.1}$$

We assume for simplicity that I has equal dimensions in the x, y, and z directions and that N is even. For ω_x, ω_y, and ω_z that are sampled on the Cartesian grid $(\omega_x,\omega_y,\omega_z) = (m,k,l)$, $m,k,l = -(M/2),\ldots,(M/2)-1$, the Fourier transform in (2.1) has the form

$$\begin{aligned}\hat{I}_{\mathrm{Cart}}(m,k,l) &\triangleq \hat{I}(m,k,l)\\ &= \sum_{u,v,w=-N/2}^{N/2-1} I(u,v,w)\\ &\quad \times e^{-\frac{2\pi i}{M}(um+vk+wl)} \end{aligned} \tag{2.2}$$

where $m,k,l = -(M/2),\ldots,(M/2)-1$, which is usually referred to as the 3-D DFT of the volume I. The parameter M $(M \geq N)$ sets the frequency resolution of the DFT. It is well known that the DFT of I, given by (2.2), can be computed in $O(M^3 \log M)$ operations.

For some applications, it is desirable to compute the Fourier transform of I in spherical coordinates. Formally, we want to sample the Fourier transform in (2.1) on the grid $(\omega_x,\omega_y,\omega_z)$ where

$$\begin{aligned}&\omega_x = r_m \cos\theta_k \sin\phi_l, \quad \omega_y = r_m \sin\theta_k \sin\phi_l\\ &\omega_z = r_m \cos\phi_l\\ &r_m = m, \quad \theta_k = 2\pi k/K, \quad \phi_l = \pi l/L\\ &m = 0,\ldots,M-1, \quad k = 0,\ldots,K-1\\ &l = 0,\ldots,L-1. \end{aligned} \tag{2.3}$$

The Fourier transform of I in spherical coordinates has the form

$$\begin{aligned}\hat{I}_{sph}(m,k,l) &\triangleq \sum_{u,v,w=-N/2}^{N/2-1} I(u,v,w)\\ &\quad \times e^{-\frac{2\pi i m}{M}(u\cos\theta_k \sin\phi_l + v\sin\theta_k \sin\phi_l + w\cos\phi_l)}. \end{aligned} \tag{2.4}$$

The spherical grid in (2.3) is equally spaced in both the radial and angular directions

$$\Delta r = r_{m+1} - r_m = 1, \quad \Delta\theta = \theta_{k+1} - \theta_k = \frac{2\pi}{K}$$
$$\Delta\phi = \phi_{l+1} - \phi_l = \frac{\pi}{L}.$$

The PPFT3D [19] evaluates the 3-D Fourier transform of a volume on the 3-D pseudopolar grid, which approximates the 3-D spherical grid, given in (2.3). Formally, the 3-D pseudopolar grid is given by the set of samples

$$P \triangleq P_1 \cup P_2 \cup P_3 \tag{2.5}$$

where

$$P_1 \triangleq \left\{\left(m, -\frac{2k}{N}m, -\frac{2l}{N}m\right)\right\}$$
$$P_2 \triangleq \left\{\left(-\frac{2k}{N}m, m, -\frac{2l}{N}m\right)\right\}$$
$$P_3 \triangleq \left\{\left(-\frac{2k}{N}m, -\frac{2l}{N}m, m\right)\right\} \tag{2.6}$$

and $k, l = -(N/2), \ldots, (N/2)$, $m = -(3N/2), \ldots, (3N/2)$. See Fig. 1 for an illustration of the sets P_1, P_2, and P_3. We define the 3-D pseudopolar Fourier transform of I as the samples of the Fourier transform $\hat{I}$, given in (2.1), on the 3-D pseudopolar grid P, given by (2.5) and (2.6). Formally, the 3-D pseudopolar Fourier transform, denoted by $\hat{I}^s_{PP}$ ($s = 1, 2, 3$), is a linear transformation, which is defined for $m = -(3N/2), \ldots, (3N/2)$ and $k, l = -(N/2), \ldots, (N/2)$ as

$$\begin{aligned}\hat{I}^1_{PP}(m,k,l) &\triangleq \hat{I}\left(m, -\frac{2k}{N}m, -\frac{2l}{N}m\right)\\ &= \sum_{u,v,w=-N/2}^{N/2-1} I(u,v,w)\\ &\quad \times e^{-\frac{2\pi i}{M}\left(mu - \frac{2k}{N}mv - \frac{2l}{N}mw\right)}\end{aligned} \tag{2.7}$$

$$\begin{aligned}\hat{I}^2_{PP}(m,k,l) &\triangleq \hat{I}\left(-\frac{2k}{N}m, m, -\frac{2l}{N}m\right)\\ &= \sum_{u,v,w=-N/2}^{N/2-1} I(u,v,w)\\ &\quad \times e^{-\frac{2\pi i}{M}\left(-\frac{2k}{N}mu + mv - \frac{2l}{N}mw\right)}\end{aligned} \tag{2.8}$$

$$\begin{aligned}\hat{I}^3_{PP}(m,k,l) &\triangleq \hat{I}\left(-\frac{2k}{N}m, -\frac{2l}{N}m, m\right)\\ &= \sum_{u,v,w=-N/2}^{N/2-1} I(u,v,w)\\ &\quad \times e^{-\frac{2\pi i}{M}\left(-\frac{2k}{N}mu - \frac{2l}{N}mv + mw\right)}\end{aligned} \tag{2.9}$$

where $\hat{I}$ is given by (2.1).

As we can see from Fig. 1, for fixed angles k and l, the samples of the 3-D pseudopolar grid are equally spaced in the radial direction. However, this spacing is different for different angles. Also, the grid is not equally spaced in the angular direction but has equally spaced slopes.

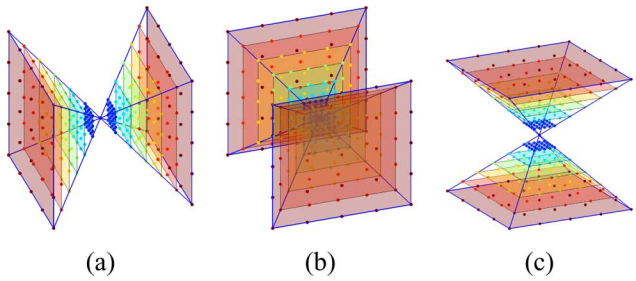

Fig. 1. The 3-D pseudopolar grid. (a) 3-D pseudopolar sector P_1; (b) 3-D pseudopolar sector P_2; and (c) 3-D pseudopolar sector P_3.

The set P, given by (2.5), can be written in polar coordinates as

$$P = \{(r\cos\theta\sin\phi, r\sin\theta\sin\phi, r\cos\phi) | (r,\theta,\phi) \in \Gamma\} \tag{2.10}$$

where the set Γ contains all triplets that correspond to points on the pseudopolar grid P.

Two important properties of the 3-D pseudopolar Fourier transform are that it is invertible and that both the forward and inverse pseudopolar Fourier transforms can be implemented using fast algorithms. Moreover, the implementations require only 1-D equispaced FFTs. In particular, the algorithms do not require regridding or interpolation.

The algorithm for computing the 3-D pseudopolar Fourier transform is based on the fractional Fourier transform. The fractional Fourier transform [20], with its generalization given by the chirp z-transform [21], is an algorithm that evaluates the Fourier transform of a sequence X on any set of N equally spaced points on the unit circle. Specifically, given a vector X of length N, $X = (X(u), u = -N/2, \ldots, N/2-1)$, and an arbitrary $\alpha \in \mathbb{R}$, the fractional Fourier transform is defined as

$$(\mathcal{F}^\alpha X)(k) = \sum_{u=-N/2}^{N/2-1} X(u) e^{-2\pi i \alpha k u/N},\ k = -N/2, \ldots, N/2. \tag{2.11}$$

The fractional Fourier transform samples the spectrum of X at the frequencies $\omega_k = \alpha k$, $k = -N/2, \ldots, N/2$, and its complexity for a given vector X of length N and an arbitrary $\alpha \in \mathbb{R}$ is $O(N \log N)$ operations.

The algorithm for computing the 3-D pseudopolar Fourier transform samples the Fourier transform of a volume I on the pseudopolar grid, with arbitrary frequency resolution in the radial and angular directions. The algorithm we present uses frequency resolution of $3N+1$ in the radial direction and $N+1$ in the angular directions. Denote the following.

- E: zero padding operator that accepts a volume I of size $N \times N \times N$ and zero pads it to size $(3N+1) \times N \times N$ (along the x direction).
- $\mathcal{F}_1$: 1-D DFT.
- $\mathcal{F}_3$: 3-D DFT.
- $\mathcal{F}^\alpha$: fractional Fourier transform with factor α. The operator $\mathcal{F}^\alpha$ accepts a sequence of length N, pads it symmetrically to length $3N+1$, applies to it the fractional Fourier

transform with factor α, and returns the $N+1$ central elements.
- $G_{k,n} \triangleq \mathcal{F}^{2k/n} \circ \mathcal{F}_1^{-1}$.

Using this notation, the algorithm for computing $\hat{I}^1_{PP}$, given by (2.7), is given in Algorithm 1. The algorithm for computing $\hat{I}^2_{PP}$ and $\hat{I}^3_{PP}$, given by (2.8) and (2.9), is similar. The complexity of the algorithm for computing $\hat{I}^1_{PP}$ (Algorithm 1) is $O(N^3 \log N)$. Since the complexity of computing $\hat{I}^2_{PP}$ and $\hat{I}^3_{PP}$ is also $O(N^3 \log N)$, the total complexity of computing the 3-D pseudopolar Fourier transform is $O(N^3 \log N)$.

Algorithm 1: Computing the 3-D Pseudopolar Fourier Transform

1: Let $\widehat{I}_d \leftarrow \mathcal{F}_3(E(I))$.
2: For each m and k set $U \leftarrow \widehat{I}_d(m,k,\cdot)$ and compute $T_1(m,k,\cdot) \leftarrow G_{k,n}(U)$.
3: For each m and l set $V \leftarrow T_1(m,\cdot,l)$ and compute $T_1'(m,\cdot,l) \leftarrow G_{k,n}(V)$.
4: For each m,k,l set $\hat{I}^1_{PP}(m,k,l) \leftarrow T_1'(m,-k,-l)$.

III. Euler's Theorem and 3-D Rotation Estimation

Rotations in a 3-D Cartesian coordinate system may be represented by various formulations. In this paper, we adopt the Euler angles representation [22], where 3-D rotations are expressed using three angles (α,β,γ), where α and β specify the direction of the rotation axis and γ specifies the angle of rotation in the plane perpendicular to the rotation axis. We denote the rotation axis by $\vec{n} \triangleq (n_x,n_y,n_z)$.

In Euler's rotation theorem, an arbitrary 3-D rotation can be expressed as a rotation by an angle γ around an axis given by a unit vector $\vec{n} = (n_x,n_y,n_z)$.

The rotation matrix R is given by

$$R = I\cos\gamma + (1-\cos\gamma)\begin{bmatrix} n_x^2 & n_xn_y & n_xn_z \\ n_yn_x & n_y^2 & n_yn_z \\ n_zn_x & n_zn_y & n_z^2 \end{bmatrix} + \sin\gamma\begin{bmatrix} 0 & -n_z & n_y \\ n_z & 0 & -n_x \\ -n_y & n_x & 0 \end{bmatrix} \quad (3.1)$$

(see [22]), where I is the identity matrix. This representation of R is not unique. The same rotation can also be obtained by a rotation of $(-\gamma)$ around the axis $(-\vec{n})$ [22]. Both γ and $\vec{n}$ can be easily recovered from the rotation matrix R. The three eigenvalues of R are $\lambda_1 = 1$ and $\lambda_{2,3} = e^{\pm i\gamma}$. The rotation axis $\vec{n}$ can be computed as $\vec{n} = \vec{v}/|\vec{v}|$, where $\vec{v}$ is the eigenvector that corresponds to λ_1, and γ can be recovered from $\lambda_{2,3}$. Any point on the rotation axis $\vec{n}$ is invariant under R, as it is also an eigenvector of R. The rotation axis $\vec{n}$ can be recovered by finding the vector where the difference between the volume and its rotated replica is minimal. Given volumes V_1 and V_2, where $V_1(x) = V_2(Rx)$, the rotation axis, given by the angles (α,β,γ), can be recovered by computing

$$\Delta V(\theta,\phi) = \int_0^\infty |V_1(r,\theta,\phi) - V_2(r,\theta,\phi)|\, dr \quad (3.2)$$

where $V_1(r,\theta,\phi)$ and $V_2(r,\theta,\phi)$ are the representations of V_1 and V_2 in spherical coordinates, and finding (α,β) such that

$$(\alpha,\beta) = \arg\min_{\theta,\phi} \Delta V(\theta,\phi). \quad (3.3)$$

For noncentered rotations, where the volumes V_1 and V_2 are translated and rotated, (3.2) is applied to the magnitudes of the Fourier transforms of V_1 and V_2, denoted M_1 and M_2, respectively. Based on the phase shift property of the Fourier transform [23], the magnitudes M_1 and M_2 are related by a three-dimensional rotation

$$M_1(R_n\vec{x}) = M_2(R_{z,\gamma}R_n\vec{x}) \quad (3.4)$$

where R_n is a 3-D rotation that aligns $\vec{n}$ with the z axis and $R_{z,\gamma}$ is a rotation of angle γ around the z axis. Thus, given the volumes V_1 and V_2, where V_1 is a rotated and translated replica of V_2, we register V_1 and V_2 using Algorithm 2.

Algorithm 2: Volume Registration

1: Let M_1 and M_2 be the magnitudes of the Fourier transform of V_1 and V_2, respectively
$$M_1 = |\mathcal{F}(V_1)|, \qquad M_2 = |\mathcal{F}(V_2)| \quad (3.5)$$
where the modulus is taken element-wise.
2: The rotation axis $\vec{n}$ is recovered by computing $\Delta V(\theta,\phi)$, given by (3.2), and locating its minimum (α,β), which corresponds to the Euler angles that define the rotation axis $\vec{n}$.
3: Given the rotation axis $\vec{n}$, we denote by $\tilde{R}$ the rotation that aligns $\vec{n}$ with the z axis. Denote
$$\tilde{M}_1 = \mathcal{F}\left(V_1(\tilde{R}\vec{x})\right), \qquad \tilde{M}_2 = \mathcal{F}\left(V_2(\tilde{R}\vec{x})\right). \quad (3.6)$$
$\tilde{M}_1$ and $\tilde{M}_2$ are related by a planar rotation of angle γ around the z axis, which can be recovered by the cylindrical motion estimation scheme described in Section IV.
4: Given the rotation parameters (α,β,γ), the 3-D rotation matrix R is computed using (3.1) and is applied to V_2. $V_1(\vec{x})$ and $V_2(R\vec{x})$ are related by a 3-D translation, which is recovered by using phase correlation (Section V).

We propose a fast and algebraically accurate scheme for the computation of ΔV in step 2, which is based on PPFT3D [19] presented in Section II. An important property of $\Delta V(\theta,\phi)$, given by (3.2), is that it can be discretized using very general

sampling grids with respect to θ and ϕ. Specifically, the discretization of ΔV, denoted by ΔV^d, does not require a uniform spherical representation of the Fourier transforms of V_1 and V_2. All that is required is a grid on which we can efficiently evaluate the Fourier transform of a given volume and whose samples lie along rays. The 3-D pseudopolar Fourier transform provides such a grid, with uniform radial sampling along each ray. Thus, the algorithm for computing ΔV^d is as follows.

Algorithm 3: Computing $\Delta V^{\mathbf{d}}(\theta, \phi)$

1: Compute M_1^d and M_2^d

$$M_1^d = |\mathcal{F}_{PP}(V_1)|, \qquad M_2^d = |\mathcal{F}_{PP}(V_2)| \tag{3.7}$$

where $\mathcal{F}_{PP}$ is the 3-D pseudopolar Fourier transform defined in Section II.

2: Evaluate (3.2) by

$$\Delta V^d(\theta_i, \phi_j) = \sum_{0 \le r_k \le \frac{M}{2}} \left| M_1^d(r_k, \theta_i, \phi_j) - M_2^d(r_k, \theta_i, \phi_j) \right| \Delta r_{i,j} \tag{3.8}$$

where M_1^d and M_2^d are given by (3.7), M is the radial resolution of the pseudopolar grid, and $\Delta r_{i,j}$ is the radial sampling interval of the 3-D pseudopolar grid for the ray whose direction is specified by θ_i and ϕ_j. Equation (3.8) is evaluated for all θ_i and ϕ_j such that $(r, \theta_i, \phi_j) \in \Gamma$ for some r, where Γ is given by (2.10).

In other words, (3.8) is evaluated for all directions of the 3-D pseudopolar grid. Different rays in the 3-D pseudopolar grid have different sampling intervals $\Delta r_{i,j}$. Equation (3.8) uses only samples of the 3-D pseudopolar Fourier transform that lie within a sphere of radius $M/2$. This summation ignores samples whose radius is in the interval $[(M/2), (\sqrt{2}M/2)]$. This interval is located at the high frequency range, as for natural volumes, the magnitude of the 3-D pseudopolar Fourier transform in this frequency range is usually negligible.

A. The Normalized Correlation Measure

The rotation axis is recovered (step 2 of Algorithm 2) by comparing corresponding rays in a spherical representation of the Fourier transforms of the registered volumes (denoted M_1^d and M_2^d in Algorithm 3). The most similar pair of corresponding rays is shown by (3.2) to correspond to the rotation axis $\vec{n}$. This similarity is measured in Algorithm 3 and (3.2) using the L_1 norm. Yet, in order to improve the robustness of our scheme with respect to noise and intensity changes, we replace the L_1 norm in (3.8) with the normalized correlation [24], which is more robust.

The normalized correlation, denoted ΔV_N^d, of two rays $M_1^d(r_k, \theta_i, \phi_j)$ and $M_2^d(r_k, \theta_i, \phi_j)$ (3.5) is given by

$$V_N^d(\theta_i, \phi_j) \triangleq \frac{\sum_{0 \le r_k \le \frac{M}{2}} \overline{M_1^d}(r_k, \theta_i, \phi_j) \overline{M_2^d}(r_k, \theta_i, \phi_j)}{\sigma_1(\theta_i, \phi_j) \sigma_2(\theta_i, \phi_j)} \tag{3.9}$$

where we have the equation shown at the bottom of the page. $N(\theta_i, \phi_j)$ is the number of samples of the pseudopolar grid with direction (θ_i, ϕ_j) whose radius is less than $M/2$ and M is the radial resolution of the 3-D pseudopolar grid. $\overline{M_l^d}$ is a zero-mean replica of M_l^d and σ_l is its standard deviation.

Equation (3.9) is evaluated for all θ_i and ϕ_j such that $(r, \theta_i, \phi_j) \in \Gamma$ for some r, where Γ is given by 2.10. The normalized correlation is more robust than the L_1 norm since it normalizes differences in the mean and standard deviation. For our application, its superiority over 3.2 is verified experimentally in Section VI. An example of ΔV_N^d (3.9) for the Skull volume [Fig. 4(e)] is depicted in Fig. 2. Fig. 2(a) shows ΔV_N^d, where the maximum is clearly visible and detectable. Fig. 2(b) shows the small support of the maximum of ΔV_N^d and demonstrates the advantages of using the 3-D pseudopolar Fourier transform.

IV. Planar Rotation

Given the rotation axis $\vec{n}$, computed by (3.2) and (3.3), we use (3.4) to rotate V_1 and V_2 [Fig. 3(a) and (b)] such that the rotation axis $\vec{n}$ is parallel to the z axis (Fig. 3(c) and (d)). This results in translated and rotated volumes, whose relative rotation is around the z axis.

Given two vectors $\vec{u}_1, \vec{u}_2 \in \mathbb{R}^3$, a 3-D rotation that transforms $\vec{u}_1$ to $\vec{u}_2$ is given by $\widetilde{R} = (\vec{u}, \psi)$, where $\psi = \arccos(\vec{u}_1 \cdot \vec{u}_2 / \|\vec{u}_1\| \|\vec{u}_2\|)$ is the rotation angle and $\vec{u} = \vec{u}_1 \times \vec{u}_2$ is the rotation axis. In order to align the rotation axis with the z axis, we set $\vec{u}_1 = (0, 0, 1)$, compute $\vec{u}_2$ using (3.3), and use ψ and $\vec{u}$ to compute the rotation matrix $\tilde{R}$.

We apply $\tilde{R}$ to V_1 and V_2 and denote the resulting volumes by $\widetilde{V}_1$ and $\widetilde{V}_2$, respectively. $\widetilde{V}_1$ and $\widetilde{V}_2$ are related by a translation and a planar rotation of angle γ around the z axis [see Fig. 3(c) and (d)]. It is possible to estimate the planar rotation by using any corresponding pair of planes in $\widetilde{V}_1$ and $\widetilde{V}_2$ that are perpendicular to the z axis [14], [25]. However, we improve the robustness of the estimate by extending the image registration

$$\overline{M_l^d}(r_k, \theta_i, \phi_j) \triangleq M_l^d(r_k, \theta_i, \phi_j) - \frac{1}{N(\theta_i, \phi_j)} \sum_{0 \le r_m \le \frac{M}{2}} M_l^d(r_m, \theta_i, \phi_j), \qquad l = 1, 2$$

$$\sigma_l(\theta_i, \phi_j) \triangleq \sqrt{\frac{1}{N(\theta_i, \phi_j)} \sum_{0 \le r_k \le \frac{M}{2}} \left(M_i^d(r_k, \theta_i, \phi_j) - \overline{M_i^d}(r_k, \theta_i, \phi_j) \right)^2}, \qquad l = 1, 2$$

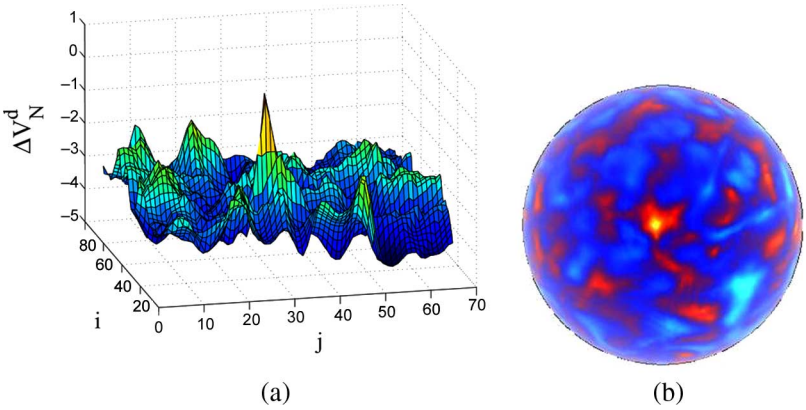

Fig. 2. Applying the normalized correlation measure to compute ΔV_N^d of the Skull volume [Fig. 4(e)] and its rotated replica. (a) The normalized correlation of ΔV_N^d. (b) ΔV_N^d overlaid on a sphere. The "hot" values correspond to the maximum. Notice its small angular support.

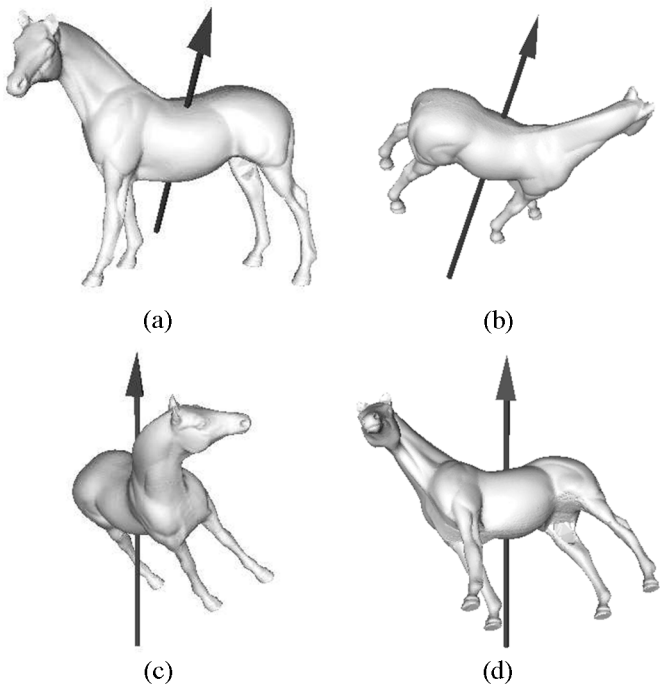

Fig. 3. Alignment of the rotation axis. The volumes in (a) and (b) are the input volumes, which are related by a rotation around the rotation axis. After recovering the rotation axis, the volumes are rotated such that the rotation axis is parallel to the z axis. Thus, the volumes in (c) and (d) are related by a translation and a planar rotation around the z axis.

scheme in [1] to cylindrical coordinates. We define the cylindrical Fourier transform of a volume V, denoted $\mathcal{F}^C$, by

$$\mathcal{F}^C(V) = \mathcal{F}_P\left(\mathcal{F}_{1D}^z\left(V(x,y,z)\right)\right) \tag{4.1}$$

where $\mathcal{F}_{1D}^z$ is the 1-D Fourier transform in the z direction and $\mathcal{F}_P$ is the 2-D polar Fourier transform, which operates on each plane that is perpendicular to the z axis.

Given two volume $\tilde{V}_1$ and $\tilde{V}_2$, which are related by a 3-D translation and a relative rotation of angle γ around the z axis, we denote

$$\tilde{M}_1 = \left|\mathcal{F}^C(\tilde{V}_1)\right|, \quad \tilde{M}_2 = \left|\mathcal{F}^C(\tilde{V}_2)\right|. \tag{4.2}$$

$\tilde{M}_1$ and $\tilde{M}_2$ are related by a planar rotation around the z axis, with no relative translation. In other words, each xy plane in $\tilde{M}_1$ is a rotated replica of the corresponding plane in $\tilde{M}_2$, i.e.,

$$\tilde{M}_1(r,\varphi,\omega_z) = \tilde{M}_2(r,\varphi+\gamma,\omega_z) \tag{4.3}$$

where r and φ are 2-D polar coordinates and γ is the relative planar rotation of the input volumes V_1 and V_2 around the rotation axis $\vec{n}$ (see Section III). The relative rotation γ is recovered by finding the minimum of

$$\Delta\tilde{M}(\varphi) = \int_0^{\pi}\int_0^{\pi}\left|\tilde{M}_1(r,\varphi,\omega_z) - \tilde{M}_2(r,-\varphi,\omega_z)\right| dr d\omega_z. \tag{4.4}$$

As shown in [1], $\Delta\tilde{M}$ is minimal when $\varphi = -\gamma/2$. Equation (4.4) uses the magnitudes of the Fourier transforms, and therefore, due to conjugate symmetry, the rotation angle can be either γ or $\gamma+\pi$. This ambiguity is resolved in Section V.

Equation (4.1) is discretized by applying the 1-D FFT in the z direction followed by computing the 2-D pseudopolar Fourier transform of each xy plane. The angular axis in (4.4) is reversed by applying a left-to-right flip on each xy plane.

V. 3-D Translation Estimation

Given the rotation parameters (α,β,γ), the 3-D rotation matrix R is computed by using (3.1). Let $\tilde{V}_2(\vec{x}) = V_2(R\vec{x})$. V_1 and $\tilde{V}_2$ are related by a 3-D translation, which is recovered by using the phase-correlation algorithm [14], [15]. As explained in Section IV, we recover the planar rotation γ by using the magnitude of the cylindrical Fourier transform. Therefore, we get that both γ and $\gamma+\pi$ are possible solutions for the planar rotation. To find the correct planar rotation, we rotate the original volume V_2 by both (α,β,γ) and $(\alpha,\beta,\gamma+\pi)$ and recover the translation by using the phase correlation. The value of the phase correlation function for each set of rotation parameters measures the quality of the alignment. Therefore, the correct planar rotation is the angle that corresponds to the higher value of the phase correlation function. The accuracy of the phase correlation scheme is limited to integer values. Subpixel accuracy and improved robustness to noise can be achieved by applying [26].

TABLE I
REGISTRATION RESULTS THAT WERE OBTAINED BY USING THE L_1 DISTANCE ΔV^d FOR THE VOLUMES SHOWN IN FIG. 4. COLUMNS 1 THROUGH 3 PRESENT THE ACTUAL ROTATION PARAMETERS. COLUMNS 4 THROUGH 6 PRESENT THE ESTIMATED ROTATION PARAMETERS. COLUMNS 7 THROUGH 9 PRESENT THE ESTIMATION ERRORS. ALL VOLUMES ARE OF SIZE $64 \times 64 \times 64$

	Actual parameters			Estimated parameters			Estimation errors		
	α	β	γ	α	β	γ	$\lvert\varepsilon_\alpha\rvert$	$\lvert\varepsilon_\beta\rvert$	$\lvert\varepsilon_\gamma\rvert$
Human Head	82.89	45.00	28.21	83.39	47.81	28.11	0.50	2.81	0.10
	80.98	25.84	44.50	80.36	25.11	44.80	0.62	0.73	0.30
	12.02	15.11	78.47	11.89	15.70	79.42	0.13	0.59	0.95
Engine	82.89	45.00	28.21	81.37	43.19	27.78	1.51	1.80	0.42
	80.98	25.84	44.50	80.78	24.15	44.86	0.19	1.68	0.36
	12.02	15.11	78.47	12.88	15.67	76.94	0.86	0.56	1.52
Spine	82.89	45.00	28.21	84.46	43.76	26.36	1.57	1.23	1.84
	80.98	25.84	44.50	80.07	27.21	44.33	0.90	1.37	0.16
	12.02	15.11	78.47	11.03	13.80	79.94	0.98	1.30	1.47
Skull	82.89	45.00	28.21	84.35	43.68	29.94	1.46	1.31	1.73
	80.98	25.84	44.50	79.90	27.81	43.55	1.0	1.97	0.94
	12.02	15.11	78.47	13.23	14.86	77.11	1.21	0.24	1.35
feet	82.89	45.00	28.21	84.52	44.36	29.70	1.63	0.63	1.49
	80.98	25.84	44.50	79.90	25.09	43.45	1.0	0.74	1.0
	12.02	15.11	78.47	10.97	14.57	79.05	1.0	0.53	0.58

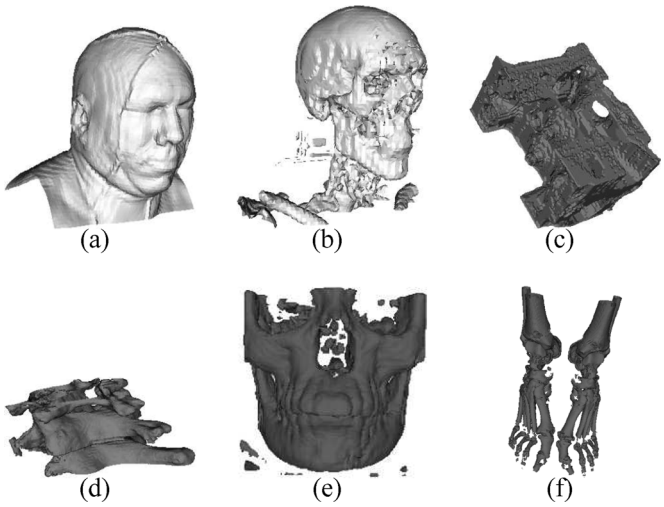

Fig. 4. Volumes that are used to evaluate the performance of the algorithm. (a) and (b) are different isosurface visualizations of the same magnetic resonance imaging (MRI) scan of a human head. (c) A computer-aided design generated model of an engine. (d) An MRI scan of a human spine. (e) A computed tomography scan of a human skull. (f) An MRI scan of human feet.

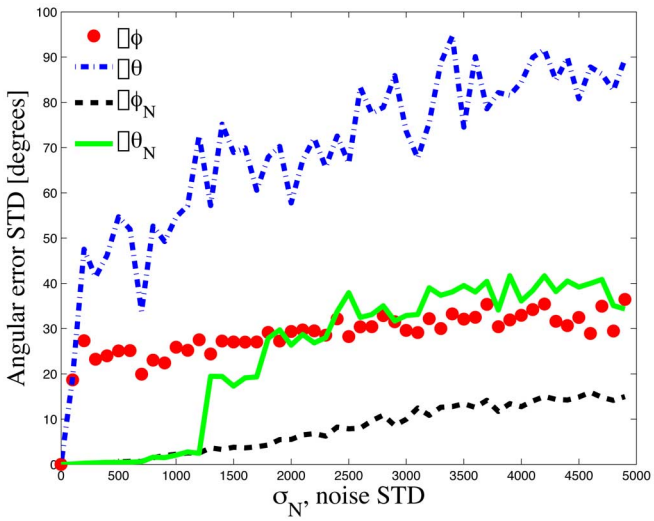

Fig. 5. The angular registration error as a function of the standard deviation of the noise. $\Delta\alpha$ and $\Delta\beta$ are the errors in the estimation of the rotation axis when using the L_1 norm (ΔV^d). $\Delta\alpha_N$ and $\Delta\beta_N$ are the estimation errors when using the normalized correlation (ΔV_N^d). Using ΔV_N^d results in improved accuracy, especially for noisy volumes.

VI. EXPERIMENTAL RESULTS

The proposed algorithm was applied to the volumes shown in Fig. 4. For each input volume, a set of rotated and translated replicas was created using bilinear interpolation, without applying any other processing such as smoothing or denoising. All volumes are of size 64^3 voxels, and the average spacing of the 3-D pseudopolar grid is $\Delta\theta = 90°/2N = 0.7°$ and $\Delta\phi = 180°/N = 1.4°$, $N = 64$. The translations are randomly chosen in the range of $[-10,10]$ pixels in each direction. Neither the accuracy of the translation estimation nor the resolving between γ and $\gamma + \pi$ is presented, since they are computed by a straightforward implementation of the 2-D phase-correlation algorithm and are not the focal point of this paper.

The results, given in Table I, show the accuracy of the proposed algorithm in noise-free settings. In all cases, the registration accuracy is on the order of the angular spacing of the 3-D pseudopolar grid. The accuracy of the registration is the same for all volumes.

Fig. 5 presents the performance of the algorithm in noisy situations. The figure shows the standard deviations (STDs) of the angular registration errors as a function of σ_n, the STD of the additive white Gaussian noise. The results are computed by adding noise to the Head and Skull volumes, shown in Fig. 4(a) and (e), respectively. Obviously, different noise realizations were added to the original volume and to its rotated replica. For each noise level σ_n, we average the alignment error over the two sets of registered volumes. It follows that for nonnoisy input volumes, the accuracy of the proposed algorithm is in the range of 0–1°, which corresponds to the average angular spacing of the 3-D pseudopolar grid. As we can see from Fig. 5, the normalized correlation ΔV_N^d (3.9) is less sensitive to additive noise. Up to $\sigma_n = 200$, the scheme is not affected by noise, and from that

TABLE II
TIMING RESULTS OF THE PROPOSED SCHEME

Volume size	$16 \times 16 \times 16$	$32 \times 32 \times 32$	$64 \times 64 \times 64$
Timing [s]	11	43	480

point on, its accuracy degrades. The nonnormalized ΔV^d, given by 3.8, achieves an accuracy better than 1° for nonnoisy volumes and then degrades. To conclude, the proposed algorithm is capable of giving reasonable estimates in extremely noisy situations.

The proposed algorithm was implemented in Matlab, and the registration times are given in Table II. The simulations were executed on a 2.8 GHz Pentium computer running WinXP. As the scheme is noniterative, these timings are invariant to the content of the registered volumes.

VII. SUMMARY AND CONCLUSIONS

This paper presents a general-purpose volume registration algorithm, which operates in the frequency domain and solves the alignment problem by computing a radial distance measure in two and three dimensions. By using Euler's theorem, the original problem, which involves six parameters, is decoupled into three subproblems: estimating the rotation axis, estimating the planar rotation, and computing the translation. The computation is based on the 2-D and 3-D pseudopolar Fourier transforms, which are fast and accurate. Compared to other schemes, we provide accurate results that are robust to noise and have a predictable execution time and controlled error.

Future work includes the registration of biological data, which is often noisy and can therefore benefit from the scheme's robustness to noise. We currently study the analysis of 3-D symmetries, which is a fundamental task in 3-D modeling and analysis. Symmetry axes can be considered as the multiple solutions of the registration of a symmetric object with itself. We have successfully applied a similar approach to images in [27].

REFERENCES

[1] Y. Keller, Y. Shkolnisky, and A. Averbuch, "The angular difference function and its application to image registration," *IEEE Trans. Pattern Anal. Mach. Intell.*, vol. 27, pp. 969–976, Jun. 2005.

[2] J. Wyngaerd and L. Van Gool, "Automatic crude patch registration: toward automatic 3D model building," *Computer Vision and Image Understanding*, vol. 87, no. 1–3, pp. 8–26, Jul. 2002.

[3] R. Benjemaa and F. Schmitt, "Fast global registration of 3D sampled surfaces using a multi-Z-buffer technique," in *Int. Conf. Recent Adv. 3D Digital Imag. Model.*, 1997, pp. 113–120.

[4] G. Papaioannou, E.-A. Karabassi, and T. Theoharis, "Reconstruction of three-dimensional objects through matching of their parts," *IEEE Trans. Pattern Anal. Mach. Intell.*, vol. 24, pp. 114–124, Jan. 2002.

[5] M. Rodrigues, R. Fisher, and Y. Liu, "Introduction: Special issue on registration and fusion of range images," *Comput. Vision Image Understand.*, vol. 87, pp. 1–7, 2002.

[6] J. A. Kovacs, P. Chacón, Y. Cong, E. Metwally, and W. Wriggers, "Fast rotational matching of rigid bodies by fast Fourier transform acceleration of five degrees of freedom," *Acta Cryst.*, vol. D59, no. 2, pp. 1371–1376, 2003.

[7] E. Katchalski-Katzir, I. Shariv, M. Eisenstein, A. A. Friesem, C. Aflalo, and I. A. Vakser, "Molecular surface recognition: Determination of geometric fit between proteins and their ligands by correlation techniques," in *Proc. Nat. Acad. Sci.*, Mar. 1992, vol. 89, pp. 2195–2199.

[8] P. J. Besl and N. D. McKay, "A method for registration of 3-D shapes," *IEEE Trans. Pattern Anal. Mach. Intell.*, vol. 14, pp. 239–255, Feb. 1992.

[9] T. Pajdla and L. Van Gool, "Matching of 3-D curves using semi-differential invariants," in *Proc. IEEE Int. Conf. Computer Vision*, Cambridge, MA, 1995, pp. 390–395.

[10] G. C. Sharp, S. W. Lee, and D. K. Wehe, "ICP registration using invariant features," *IEEE Trans. Pattern Anal. Mach. Intell.*, vol. 24, pp. 90–102, Jan. 2002.

[11] L. Lucchese, G. Doretto, and G. Cortelazzo, "A frequency domain technique for range data registration," *IEEE Trans. Pattern Anal. Mach. Intell.*, vol. 24, no. 11, pp. 1468–1484, 2002.

[12] P. Thévenaz, U. Ruttimann, and M. Unser, "A pyramid approach to subpixel registration based on intensity," *IEEE Trans. Image Process.*, vol. 7, pp. 27–41, Jan. 1998.

[13] G. M. Cortelazzo, G. Doretto, and L. Lucchese, "Free-form textured surfaces registration by a frequency domain technique," in *IEEE Int. Conf. Image Process.*, Oct. 1998, vol. 1, pp. 813–817.

[14] S. Reddy and B. N. Chatterji, "An FFT-based technique for translation, rotation, and scale-invariant image registration," *IEEE Trans. Image Process.*, no. 8, pp. 1266–1270, Aug. 1996.

[15] C. D. Kuglin and D. C. Hines, "The phase correlation image alignment method," in *IEEE Conf. Cybern. Soc.*, Sep. 1975, pp. 163–165.

[16] J. A. Kovacs, P. Chacón, Y. Cong, E. Metwally, and W. Wriggers, "Fast rotational matching of rigid bodies by fast Fourier transform acceleration of five degrees of freedom," *Acta Crystal. Sec. D*, vol. 59, no. 8, pp. 1371–1376, Aug. 2003.

[17] Y. Keller, Y. Shkolnisky, and A. Averbuch, "Algebraically accurate volume registration using Euler's theorem and the 3-D pseudo-polar FFT," in *Proc. IEEE Conf. Comput. Vision Pattern Recognit.*, Jun. 2005.

[18] A. Averbuch, D. Donoho, R. Coifman, M. Israeli, and Y. Shkolnisky, "Fast slant stack: A notion of Radon transform for data in Cartesian grid which is rapidly computable, algebrically exact, geometrically faithful and invertible," *SIAM Sci. Comput.*, to be published.

[19] A. Averbuch and Y. Shkolnisky, "3D Fourier based discrete Radon transform," *Appl. Comput. Harmon. Anal.*, vol. 15, pp. 33–69, 2003.

[20] D. H. Bailey and P. N. Swarztrauber, "The fractional Fourier transform and applications," *SIAM Rev.*, vol. 33, no. 3, pp. 389–404, September 1991.

[21] L. R. Rabiner, R. W. Schafer, and C. Rader, "The chirp z-transform algorithm," *IEEE Trans. Audio Electroacoust.*, vol. AU, no. AU0017, pp. 86–92, Jun. 1969.

[22] E. Trucco and A. Verri, *Introductory Techniques for 3-D Computer Vision*. Englewood Cliffs, NJ: Prentice-Hall, 1998, pp. 333–334.

[23] B. Porat, *A Course in Digital Signal Processing*. New York: Wiley, 1997.

[24] F. M. Dickey and L. A. Romero, "Normalized correlation for pattern recognition," *Opt. Lett.*, vol. 16, no. 15, pp. 1186–1188, Aug. 1991.

[25] P. Milanfar, "Two-dimensional matched filtering for motion estimation," *IEEE Trans. Image Process.*, vol. 8, pp. 438–443, Mar. 1999.

[26] W. S. Hoge and C.-F. Westin, "Identification of translational displacements between N-dimensional data sets using the high order SVD and phase correlation," *IEEE Trans. Image Process.*, vol. 14, pp. 884–889, Jul. 2005.

[27] Y. Keller and Y. Shkolnisky, "An algebraic approach to symmetry detection," in *Proc. 17th Int. Conf. Pattern Recognit. (ICPR 2004)*, Aug. 2004, vol. 3, pp. 186–189.

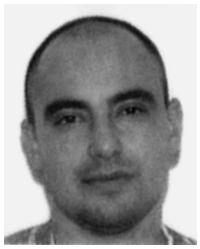

Yosi Keller received the B.Sc. degree in electrical engineering from The Technion—Israel Institute of Technology, Haifa, in 1994. He received the M.Sc and Ph.D. degrees in electrical engineering from Tel Aviv University, Tel Aviv, Israel, in 1998 and 2003, respectively.

From 1994 to 1998, he was an R&D Officer in the Israeli Intelligence Force. He is a Visiting Assistant Professor with the Department of Mathematics, Yale University. His research interests include motion estimation, video analysis, image restoration, and statistical pattern analysis.

Yoel Shkolnisky received the B.Sc. degree in mathematics and computer science and the M.Sc. degree in computer science from Tel Aviv University, Tel Aviv, Israel, in 1996 and 2001, respectively, where he is currently pursuing the Ph.D. degree.

His research interests include computational harmonic analysis and scientific computing in problems related to irregular sampling and polar processing.

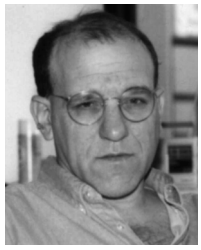

Amir Averbuch was born in Tel Aviv, Israel. He received the B.Sc. and M.Sc. degrees in mathematics from the Hebrew University. Jerusalem, Israel. in 1971 and 1975, respectively. He received the Ph.D. degree in computer science from Columbia University, New York, in 1983.

During 1966–1970 and 1973–1976, he served in the Israel Defense Forces. From 1976 to 1986 he was a Research Staff Member with the Department of Computer Science, IBM T. J. Watson Research Center, Yorktown Heights, NY. In 1987, he joined the Department of Computer Science, School of Mathematical Sciences, Tel Aviv University, where he is now a Professor of computer science. His research interests include wavelets, signal/image processing, multiresolution analysis, numerical computation for the solutions of PDEs, scientific computing (fast algorithms), and parallel and supercomputing (software and algorithms).